HHS Public Access

Author manuscript

Environ Sci Technol. Author manuscript; available in PMC 2018 June 06.

Published in final edited form as:

Environ Sci Technol. 2017 June 06; 51(11): 5978–5988. doi:10.1021/acs.est.7b00508.

Analysis of photo-irradiated water accommodated fractions of crude oils using tandem TIMS and FT-ICR MS

Paolo Benigni[1], **Kathia Sandoval**[1], **Christopher J. Thompson**[2], **Mark E. Ridgeway**[2], **Melvin A. Park**[2], **Piero Gardinali**[1,3], and **Francisco Fernandez-Lima**[1,4]

[1]Department of Chemistry and Biochemistry, Florida International University, Miami, FL 33199, USA

[2]Bruker Daltonics, Inc., Billerica, Massachusetts 01821, USA

[3]Southeast Environmental Research Center, Florida International University, Miami, Florida 33199, USA

[4]Biomolecular Sciences Institute, Florida International University, Miami, FL 33199

Abstract

For the first time, trapped ion mobility spectrometry (TIMS) in tandem with Fourier transform ion cyclotron resonance mass spectrometry (FT-ICR MS) is applied to the analysis of the low energy water accommodated fraction (WAF) of a crude oil as a function of the exposure to light. The TIMS-FT-ICR MS analysis provided, in addition to the heteroatom series identification, new insights into the WAF isomeric complexity (e.g., [*m/z*; chemical formula; collision cross section] datasets) for a better evaluation of the degree of chemical and structural photo-induced transformations. Inspection of the [*m/z*; chemical formula; collision cross section] datasets shows that the WAF composition changes as a function of the exposure to light in the first 115 hours by initial photo-solubilization of HC components and their photo-oxidation up to $O_{4–5}$ of mainly high double bond equivalence species (DBE > 9). The addition of high resolution TIMS (resolving power of 90–220) to ultrahigh resolution FT-ICR MS (resolving power over 400k) permitted the identification of a larger number of molecular components in a single analysis (e.g., over 47k using TIM-MS compared to 12k by MS alone), with instances of over 6-fold increase in the number of molecular features per nominal mass due to the WAF isomeric complexity. This work represents a stepping stone towards a better understanding of the WAF components and highlights the need for better experimental and theoretical approaches to characterize the WAF structural diversity.

[*]**Corresponding Author:** Francisco Fernandez-Lima, Phone: 305-348-2037., Fax: 305-348-3772. fernandf@fiu.edu.

Supporting Information

Additional information as noted in the text. Figure S1. Schematic of a trapped ion mobility analyzer. Figure S2. Carbon number vs DBE plot for the $O_{0–3}$ chemical classes for the WAF at t-0, 16 and 115h of exposure to light. Figure S3. Carbon number vs DBE plot for the $O_{4–5}$ chemical classes for the WAF at t-115h of exposure to light. Figure S4. Carbon number vs DBE plot for the N1O0-3 chemical classes for the WAF at t-0, 16 and 115h of exposure to light. This material is available free of charge via the Internet at http://pubs.acs.org.

Notes

The authors declare no competing financial interest.

TOC image

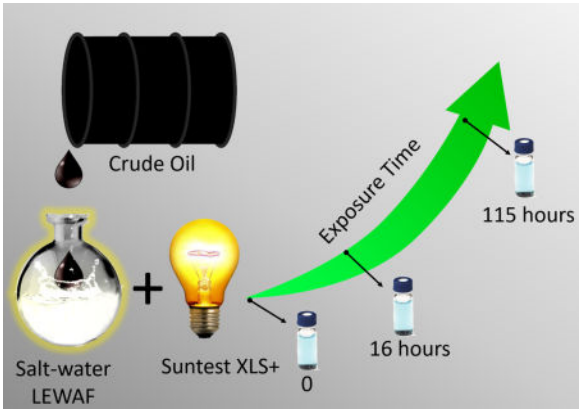

Keywords

Ion mobility spectrometry; TIMS-FT-ICR MS; IMS-MS; Polyaromatic Hydrocarbons; PAH; Water Accommodated Fraction; WAF; Oxygenation

INTRODUCTION

The complex nature of crude oil and its incorporation in aquatic systems results in complex chemical transformations mainly via bio-[1–8] and photo-degradation.[9–14] Natural and anthropogenic release of crude oil and hydrocarbons[15, 16] to seawater is a frequent process and recent studies have highlighted the importance of characterizing released crude oil at the molecular level.[17] For example, the characterization of hetero-atom (O, N, and S) poly aromatic hydrocarbons (h-PAHs) have exhibited increased levels of toxicity compared to pure hydrocarbons.[18] Moreover, PAHs are photo active, undergoing oxygenation upon exposure to light, which can lead to chemical products that have increased biological accumulation and activity.[19–25] The presence of crude oil in water provides the means for the exposure of a large number of molecules to chemical and enzymatic transformation, their transportation across environments,[26–28] as well as the interaction with a variety of organisms.[26] Many of these chemical changes, as well as the means of exposure to organisms, occur in the water accommodated fraction, where low energy mixing introduces components of the oil into the water, without the formation of detectable emulsions.[29] The main analytical challenge during the analysis of the low energy water accommodated fraction (WAF) remains the identification and quantitation of both the primary molecular species, as well as the transformation intermediates and products.

Over the past years, most of the efforts for the WAF analysis has been focused on the use of gas chromatography – mass spectrometry (GC-MS)[7, 9, 10, 13, 30–36] and two dimensional gas chromatography (GCXGC-MS) with heavy standards.[31, 37] While progress has been made in the WAF characterization, these approaches are limited to the volatility range of molecules that can be analyzed by GC, which typically excludes large and highly polar molecules.[38] These analytical limitations narrow the type of studies that can be performed and our understanding of the crude oil transformations in seawater; especially, since the molecular

species that are inaccessible or form unresolvable ‘humps’, known as the unresolved complex mixture (UCM), can make up most of the WAF content.[39, 40] The analytical challenges associated with the molecular characterization of the UCM has led to the use of alternative tools in order to unravel its chemical complexity. For example, studies utilizing ultra-high mass resolution mass spectrometry (e.g., FT-ICR MS)[41–44] have enabled the identification of chemical formulas using the isotopic resolution and the high mass accuracy (sub ppm) with a variety of atmospheric pressure ionization sources (e.g., electrospray ionization, ESI,[45, 46] atmospheric pressure chemical ionization, APCI,[47–49] atmospheric pressure photo-ionization, APPI,[50–53] and atmospheric pressure laser ionization, APLI[54–61]). The use of a variety of atmospheric pressure ionization sources has enabled, in turn, the study of different molecular fractions at the molecular level and has provided evidence of the high structural diversity of the WAF components in their functional groups, aromaticity, and polarity.[62–64]

The high structural diversity of the WAF samples has prompted the need to complement ultrahigh resolution mass analysis (e.g., FT-ICR MS measurements) with pre-separation techniques (e.g., liquid and gas chromatography), in order to better discriminate the components along a second axis of separation, permitting some isomeric separation and increasing the dynamic range of the FT-ICR MS measurement.[59, 60, 65–69] However, the biggest challenge in the coupling of liquid and gas chromatography is that it limits the FT-ICR MS analysis time, and thus the ability to better separate isobaric species, due to the slow acquisition rates needed for ultrahigh resolution mass acquisitions.[48, 65] Alternatively, other post-ionization, gas-phase separations have been proven to be a better match for FT-ICR MS analysis.[70–79] In particular, ion mobility spectrometry (IMS) presents many advantages for the analysis of complex mixtures, providing orthogonal separation to FT-ICR MS that is based on the tri-dimensional structure of the molecule.[80–82] Initial work showed the potential of IMS-MS analysis for the characterization of complex hydrocarbon mixtures using complementary IMS-MS and FT-ICR MS measurements (e.g., IMS-TOF MS and FT-ICR MS of the same sample).[83–92] More recently, with the development of trapped ion mobility spectrometry (TIMS),[93–95] several reports have shown the potential of TIMS-MS to decouple the mobility (K) separation from the MS analysis time for fast, gas-phase separation and for molecular structural elucidation.[51, 93, 96–117] In particular, the advantages of TIMS over traditional IMS analyzers has been shown for fast screening[96] and targeted[79] analysis of molecular ions from complex chemical mixtures; the study of isomerization kinetics of small molecules,[98] peptides, DNA, proteins and their complexes in the absence of the bulk solvent;[99–103] the influence of the collision partner on the molecular structure;[104] and the factors that affect molecular-adduct complex lifetime and stability during TIMS measurements.[105] A significant feature to note is the high resolving power of TIMS analyzers (R_{TIMS} up to 400[107]) and accuracy in measuring ion-neutral collision cross section (CCS, <0.6% error). In the case of crude oils and complex mixtures, their characterization by TIMS-FT-ICR MS has allowed the measurement of the CCS, accurate mass and accurate isotopic fine structure in a single experiment for a series of h-PAHs. For example, a recent report of Oversampling Selective Accumulation Trapped Ion Mobility Spectrometry (OSA-TIMS) coupled to FT-ICR MS showed high mobility resolving powers (over 250), high mass

accuracy (<1 ppm), and ultrahigh mass resolution (over 1,200,000 at *m/z* 400) during the analysis of a complex mixture of polyaromatic hydrocarbons (PAH) from coal tar.[106]

In the present work, for the first time, we apply tandem OSA-TIMS and FT-ICR MS for the analysis of WAF samples as a function to their exposure to light. While preliminary work has shown that WAF can undergo chemical and increase the solubilization as a function to the exposure to light,[43] little is known about the WAF structural variability and transformation pathways. In this study, as an initial step, the analysis focuses on the PAH compounds accessible to ionization by an APLI source (e.g., mostly conjugated molecules) which typically exhibit higher reactivity to light resulting in more hazardous byproducts.[118] In addition to the new analytical advantages of TIMS-FT-ICR MS, a Software Assisted Molecular Elucidation (SAME) package was developed for the unsupervised processing of the OSA-TIMS-FT-ICR MS datasets. As shown below, this work highlights the need for high mobility resolution and ultra-high resolution MS for the analysis of the highly isomeric, complex WAF mixtures while providing [*m/z*; chemical formula; K; CCS] in a single experiment.

EXPERIMENTAL

Sample preparation

Low-energy water accommodated fractions (WAF) were generated according to the standardized protocol established by the Chemical Response to Oil Spills: Ecological Research Forum (CROSERF).[119, 120] Briefly, WAFs were prepared at room temperature in 2-L aspirator bottles with 20% headspace by volume using artificial filtered saltwater (pore size: 0.45μm, salinity=33 parts-per-thousand) prepared with Instant Ocean® (Aquarium Systems, Mentor OH). Oil from the Marlin Platform was added to the water surface using a gastight syringe at an oil-to-water loading of 1:1000 (1 g oil/L seawater). The bottles were covered in aluminum foil and allowed to mix for 24h at low speed (100 rpm) in the dark.

WAF exposure to light and extraction

WAF samples were irradiated up to 115h with a Suntest XLS+ Sunlight Exposure System equipped with a 1500W xenon arc lamp and light intensity of 765 W/m^2 (Atlas, Chicago, IL, USA). The aspirator bottles containing the WAF and the oil were placed in a water bath system set to 25℃. At specific irradiation times (0, 16, and 115h), 150 ml aliquots of the WAF were removed and subjected to liquid-liquid extraction in three 50 mL lots of methylene chloride to increase extraction efficiency. Aliquots were dried over Na_2SO_4 and concentrated down to 1 mL under a stream of nitrogen. The final samples were then diluted 1:100 in 1:1 v/v methanol/toluene for FT-ICR MS and TIMS-FT-ICR MS analysis.

FT-ICR MS analysis

WAF samples were analyzed in positive ion mode with an APLI source coupled to a custom-built TIMS – FT-ICR MS instrument based on the 7T Solarix FT-ICR MS spectrometer (Bruker Daltonics Inc., MA). Briefly, the APLI source utilizes a 266 nm excimer laser (CryLas GmbH, Berlin, Germany; Type:1HP266-50); the sample was introduced at 200 μL/h through a short nebulizer in a vaporizer set to 300 °C into the source chamber where the gas

stream was ionized by the excimer laser.[65] The APLI generates radical ($[M]^{+\cdot}$) and protonated ($[M+H]^+$) ions in the source region that are introduced to the TIMS-FT-ICR MS via a 0.6 mm inner diameter, single-bore resistive glass capillary tube, allowing the nebulizer to be maintained at ground potential, while the ends of the capillary can be independently biased. Typical APLI operating conditions were 1 L/min dry gas flow rate, 2.1 bar nebulizer gas pressure, and 220 °C dry gas temperature. FT-ICR MS ion optics were optimized as follows: −900 V endcap source capillary voltage, 180 V endcap TIMS capillary voltage, 5kHz 400 peak-to-peak voltage (Vpp) segmented hexapole, 2kHz 1900 Vpp collision cell, and 4kHz 400 Vpp ion guide transfer line. The FT-ICR MS experiments were performed by co-adding 200 16 Megaword (8 second) transients, which were zero-filled to 32Megaword, processed using a half-sine apodization followed by fast-Fourier transform (FFT) and broadband phase correction (absorption spectra using absorption mode processing, AMP); an experimental MS resolving power with AMP at *m/z* 400 of ~2,000,000 was obtained.

TIMS-FT-ICR MS Analysis

The concept behind TIMS is the use of an electric field to hold ions stationary against a moving gas, so that the drag force is compensated by the electric field and ion packages are separated across the TIMS analyzer axis based on their mobility.[93–95] During mobility separation, a quadrupolar field confines the ions in the radial direction to increase trapping efficiency. A simplified schematic of a TIMS analyzer is shown in the Supporting Information (Figure S1). The mobility, K, of an ion in a TIMS cell is described by:

$$K = \frac{v_g}{E} = \frac{A}{(V_{elution} - V_{out})} \quad (1)$$

where v_g, E, $V_{elution}$ and V_{out} are the velocity of the gas, applied electric field, elution voltage and tunnel out voltage, respectively. TIMS separation was performed using nitrogen as a bath gas at *ca.* 300 K, front end P_1 = 3.0 and back end P_2 = 1.1 mbar pressures, a constant V_{out} = 35 V and constant RF (840 kHz and 240 Vpp) in all electrodes of the entrance funnel, mobility separating section and exit funnel. Details regarding Oversampling Selected Accumulation TIMS (OSA-TIMS) modes of operation[106] and specifics compared to traditional TIMS and IMS can be found elsewhere.[93–96, 98] Briefly, OSA-TIMS experiments were performed by scanning V_{in} from −40 to −210 V using a 1 V ramp size and 0.2 V increments per step, accumulating 40 mobility experiments per FT-ICR MS spectrum (4Megaword, 3s transient, with six transients co-added per MS). TIMS-FT-ICR MS spectra were processed using sine-squared apodization followed by FFT, in magnitude mode resulting in an experimental MS resolving power of R ~ 400,000 at *m/z* 400. Mobility spectra were calibrated using a Tuning Mix calibration standard (Tunemix, G2421A, Agilent Technologies, Santa Clara, CA) with the following reduced mobility (K_o) values *m/z* 622 K_0=1.025, *m/z* 922 K_0=0.840, *m/z* 1222 K_0=0.724¸ *m/z* 1522 K_0=0.643 $cm^2\ V^{-1}s^{-1}$. Mobilities were correlated with CCS (Ω) using the equation:

$$\Omega=\frac{(18\pi)^{1/2}}{16}\frac{z}{(k_B T)^{1/2}}\left[\frac{1}{m_I}+\frac{1}{m_b}\right]^{1/2}\frac{1}{K}\frac{760}{P}\frac{T}{273.15}\frac{1}{N^*} \quad (2)$$

where z is the charge of the ion, k_B is the Boltzmann constant, N^* is the number density and m_I and m_b refer to the masses of the ion and bath gas, respectively.[121] Under these conditions, the experimental TIMS resolving power for Tuning Mix (*m/z* 622–1522) was ~100–250 as determined by equation 3.

$$R=\frac{\Omega}{\Delta\Omega} \quad (3)$$

Data Processing

FT-ICR MS spectra were externally mass calibrated using the Tuning Mix standard. A peak list was generated allowing a signal to noise ratio of 6 and the data were internally, recalibrated (post-acquisition) using a double bond equivalence of 9 O_1 series to improve overall mass accuracy.[122] The formulae calculations from the exact mass domain were performed using Composer software (Version 1.0.6, Sierra Analytics, CA) and confirmed with Data Analysis (Bruker Daltonics v 4.2) using formula limits of $C_{1–100}H_{1–100}N_{0–2}O_{0–7}S_{0–2}$, odd and even electron configurations were allowed, and $M^{+\cdot}$ and $[M+H]^+$ ion forms. A root mean square deviation for the mass assignments of 0.3 ppm was observed. From the generated ion formulas, the double bond equivalence (DBE) was calculated by the equation:

$$DBE=C-\frac{H}{2}+\frac{N}{2}+1 \quad (4)$$

where C, H and N are the number of carbons, hydrogens, and nitrogen in the chemical formula.

The peak list was used for extraction of the ion mobility spectra from the TIMS-FT-ICR MS datasets using batch processing in the Data Analysis package (Version v. 4.2, Bruker Daltonics, CA) followed by external mobility calibration using the Tuning Mix standards. The TIMS spectrum for each molecular formula was processed using a custom-built Software Assisted Molecular Elucidation (SAME) package – a specifically designed 2D TIMS-FT-ICR MS data processing script written in Python v2.7. SAME package utilizes noise removal, mean gap filling, “asymmetric least squares smoothing” base line correction,[70] peak detection by continuous wavelet transform (CWT)-based peak detection algorithm (SciPy package),[123, 124] and Gaussian fitting with non-linear least squares functions (Levenberg-Marquardt algorithm).[125] SAME final outcome is [*m/z*; chemical formula; K; CCS] for each 2D TIMS-FT-ICR MS dataset. The 2D TIMS-FT-ICR MS

contour plots were generated in DataAnalysis (Version v. 4.2, Bruker Daltonics, CA) and all the other plots were generated using matplotlib[126] and OriginPro 2016 (Originlab Co., MA).

RESULTS AND DISCUSSION

The analysis of the WAF samples by APLI-FT-ICR MS can be characterized by a Gaussian-like distribution, centered at *m/z* 300 (Figure 1). Prior to exposure to light (t-0h), ~700 peaks were observed in the FT-ICR MS spectra. After the WAF was exposed to light (t-115h), the distribution increased in size, and the center shifted to *m/z* 500, resulting in ~ 12,000 peaks, which represents a ~17-fold increase relative to the unexposed WAF (t-0h). The change in the MS distribution suggest an increased partitioning of the oil in the WAF (e.g., photo-solubilization) as well as potential chemical transformations within the WAF as a function of the exposure to light. The use of ultra-high resolution mass analyzers allowed the assignment of chemical formulas and to follow the WAF changes as a function of the exposure to light (see Figure S2–4). A follow up analysis using OSA-TIMS in tandem with FT-ICR MS enabled further molecular separation of the WAF content by their mobility (isomeric content) followed by ultra-high resolution mass analysis. For example, the number of molecular features increased from ~700 to ~5.2 k and from ~12k to ~47k for the t-0 and t-115h WAF samples, respectively, by adding the TIMS separation to the FT-ICR MS analysis. Moreover, the isomeric content of the WAF samples is such that TIMS separation increases the number of features in up to 6-fold at the nominal mass level (see Figure 1). That is, OSA-TIMS in tandem with FT-ICR MS enabled a more comprehensive analysis of the WAF content by increasing the peak capacity of the analysis using complementary, orthogonal TIMS and FT-ICR MS separations.

Inspection of the 2D-TIMS-FT-ICR MS contour plots indicated that the observed chemical species from the WAF samples using the APLI source are mostly condensed/aromatic molecules (see more details on interpreting 2D-IMS-MS contour plots in reference[106]). This observation is consistent with previous analysis using APLI sources that showed better ionization efficiencies for molecules containing conjugated bonds.[65] Closer inspection of the 2D TIMS-FT-ICR MS WAF data reveals the spectral complexity in both the mass and mobility dimensions. Particularly, the presence of multiple isobaric interferences (e.g., -C_3 to -SH_4 splits, Δm=3.4 mDa, requiring ~150,000 resolving power at *m/z* 489), such as $C_{31}H_{37}O$, $C_{28}H_{41}OS$, and $C_{25}H_{45}OS_2$, as well as multi-band ion mobility projections confirm the need for high resolution TIMS analysis during the study of the WAF samples (TIMS resolving power up to 220 is shown in Figure 2). For example, at *m/z* 327, 14 MS peaks are detected and chemical formulas are assigned (Table 1). For each chemical formula, an extracted ion mobility chromatogram was generated, resulting on 47 peaks with assigned chemical formula, mobility and CCS. Notice that this detailed separation is only possible due to the high resolving power of the TIMS device, the OSA-TIMS method providing sufficient points across the mobility profile, and the ultra-high resolution and mass accuracy of the FT-ICR MS. Moreover, the processing of the 2D-TIMS-FT-ICR MS data using the SAME package is able to deconvolute the mobility profile in a minimum number of isomers (see example for $C_{22}H_{31}O_2^+$ and $C_{21}H_{27}O_3^+$ in Figure 2). A similar complexity can be observed at *m/z* 489, where 17 peaks are resolved in the FT-ICR MS and 123 peaks in the 2D TIMS-FT-ICR MS. The time independent nature of the OSA-TIMS analysis permits the

acquisition of high mass resolution FT-ICR MS spectra, thus maximizing the analytical potential of both techniques while providing precise collision cross section (less than 1% variability between replicates). It should be pointed out that these results provide a new reference point for the IMS-MS analysis; commonly accessible IMS-MS platforms are limited to IMS resolving power of ~30–60 (with instances up to 100) and to TOF MS detectors with MS resolving power up to 60k.[83–91]

Taking advantage of the high mobility resolution and ultra-high mass separation of TIMS-FT-ICR MS, the WAF [*m/z*; chemical formula; K; CCS] components can be followed as a function of the exposure to light for each chemical class (see example in Figure 3). The increase in the number of molecular species from the HC class as a function of the exposure to light suggest that WAF is initially subject to photo-solubilization of the surface slick into the water, in good agreement with previous observations.[41] Results show that an increase in the DBE of a molecule increases is associated with a reduction in the CCS for a given carbon number. For example, for C_{34} the lowest CCS of 210 $Å^2$ corresponds to DBE 14, while DBE 5 has the greatest CCS of 252 $Å^2$. This indicates that the degree of condensation (e.g., rings and double bonds) imposes structural boundaries, reducing the CCS of a molecule.[85, 127] In addition to the initial photo-solubilization, as the exposure of the WAF to light increases, a greater number of assignments with carbon numbers greater than 40 are observed, particularly comparing 16 and 115h. Furthermore, there is an increase in the number of oxygenated classes and a decrease in the HC class, particularly for compounds with DBE>9. In particular, the identified formulas for the O_4 and O_5 classes have DBE ranges between 8–20 and 9–18, respectively. These identified formulas occupy a narrow structural space in the condensed region of the mobility domain, which may indicate that these are products of the higher photosensitive and reactive aromatic HC structures.[128] Although the WAF transformation mechanisms are not well understood, our results suggest that the photo-transformation of the HC molecules in WAF leads to the observation of oxygenated species of the $O_{4\text{-}5}$ class in the first 115h of exposure to light.

Changes in the WAF composition can be also followed by the presence of specific chemical formulas as a function of the exposure to light. For example, inspection of the WAF [*m/z*; chemical formula; K; CCS] components at different time points can be used to infer the degree of chemical transformations (see Figure 4). For example, the unexposed WAF, t-0h, has few identifications for the HC class (black bars); however, at t-16h (red bars) there is a significant increase in the number of assignments, 420 new identifications based on MS alone and 3000 based on TIMS-MS followed by a decrease in the number of non-oxygenated molecules (e.g., HC and N class molecules) at t-115h.[43] This result suggest that there are several chemical transformations occurring as a consequence of the photo-solubilization of the surface oil (e.g., indicated by the new identifications for the HC class at t-115h) and increased oxygenation of previously dissolved WAF components (e.g., the three-fold increase in the number of identifications for the O_3 class, and the appearance of the O_4 and O_5 class with 1140 and 420 identifications, respectively). The oxygenated molecules are also highly isomeric, with up to 9 ion mobility bands per chemical formula. The observation of the $O_{4\text{-}5}$ classes at later irradiation times (t-115h) suggest that these molecules were not originally present in the WAF, but are a consequence of the oxygenation process that took place over time, either by the generation of new molecules, or by a decrease in matrix effects

due to a lower number of UV absorbent molecules. That is, a reduction of molecules that are highly absorbent of the 266 nm excimer laser may result in greater sensitivity for less absorbent and low concentration molecules. Note that the increase in oxygenation is in good agreement with other MS reports of WAF exposure to light.[129, 130] Small differences were observed between the number of identifications, such as the HC class, by TIMS-MS and MS alone due to the reduced TIMS trapping efficiency for low *m/z* ions and low abundant ions when performing a broad range mobility analysis; however, this limitation can be overcome by performing targeted analysis for smaller PAHs (e.g., naphthalene) as previously reported.[96]

While this work showcases the unique advantages of OSA-TIMS in tandem with FT-ICR MS and represents a major step towards the analytical characterization (i.e., high mobility resolving power over 220 combined with ultrahigh mass resolution over 400k) of the WAF samples at the molecular level in a single experiment, further experiments and developments are needed. For example, a more complete characterization of the WAF content and their transformation products and intermediates will require the use of a suite of ionization sources, in both positive and negative polarities, in order to cover a larger range of chemical species during the analysis.[62, 131] Further interpretation of the WAF [*m/z*; chemical formula; K; CCS] components can be made with the use of standards, theoretical calculations of candidate structures,[79, 96, 97] and the implementation of complementary, post-ionization MS structural tools in tandem with TIMS-FT-ICR MS (e.g., MS/MS using CID, SID, IRMPD, BIRD, ExD, etc.)[132–138] Although initial attempts have been made towards the structural characterization,[97] the 2D TIMS-FT-ICR MS datasets contain a large amount of analytical data (e.g., over 50k features) in need for further development of theoretical ‘petro-informatics’ and computational approaches capable of producing more detailed structural information of the WAF photo-transformation products and intermediates.

Supplementary Material

Refer to Web version on PubMed Central for supplementary material.

Acknowledgments

This work was supported by the National Institute of Health (R00GM106414), a Bruker Daltonics Inc. fellowship, and a National Science Foundation Division of Chemistry, under CAREER award CHE-1654274, with co-funding from the Division of Molecular and Cellular Biosciences to FFL. PB acknowledges the fellowship provided by the National Science Foundation award (HRD-1547798) to Florida International University as part of the Centers for Research Excellence in Science and Technology (CREST) Program. The authors would like to thank Dr. James Martin Quirke (FIU) and Dr. Steven Van Orden (Bruker Daltonics Inc.) for helpful discussions and suggestions, and acknowledge the Advance Mass Spectrometry Facility at Florida International University for their support.

References

1. Ghosal D, Ghosh S, Dutta TK, Ahn Y. Current state of knowledge in microbial degradation of polycyclic aromatic hydrocarbons (PAHs): a review. Front Microbiol. 2016; 7
2. Kanaly RA, Harayama S. Biodegradation of high-molecular-weight polycyclic aromatic hydrocarbons by bacteria. J Bacterio. 2000; 182(8):2059–2067.
3. Haritash AK, Kaushik CP. Biodegradation aspects of polycyclic aromatic hydrocarbons (PAHs): a review. J Hazard Mater. 2009; 169(1–3):1–15. [PubMed: 19442441]

4. King GM, Kostka JE, Hazen TC, Sobecky PA. Microbial responses to the Deepwater Horizon oil spill: from coastal wetlands to the deep sea. Ann Rev Mar Sci. 2015; 7(1):377–401.
5. Venosa AD, Zhu XQ. Biodegradation of crude oil contaminating marine shorelines and freshwater wetlands. Spill Sci Technol B. 2003; 8(2):163–178.
6. Wang J, Sandoval K, Ding Y, Stoeckel D, Minard-Smith A, Andersen G, Dubinsky EA, Atlas R, Gardinali P. Biodegradation of dispersed Macondo crude oil by indigenous Gulf of Mexico microbial communities. Sci Total Environ. 2016; 557–558:453–468.
7. Yang ZY, Hollebone BP, Wang ZD, Yang C, Brown C, Zhang G, Landriault M, Ruan XC. A preliminary study for the photolysis behavior of biodiesel and its blends with petroleum oil in simulated freshwater. Fuel. 2015; 139:248–256.
8. Gutierrez T, Singleton DR, Berry D, Yang T, Aitken MD, Teske A. Hydrocarbon-degrading bacteria enriched by the Deepwater Horizon oil spill identified by cultivation and DNA-SIP. ISME J. 2013; 7(11):2091. [PubMed: 23788333]
9. D'Auria M, Emanuele L, Racioppi R, Velluzzi V. Photochemical degradation of crude oil: Comparison between direct irradiation, photocatalysis, and photocatalysis on zeolite. J Hazard Mater. 2009; 164(1):32–8. [PubMed: 18768253]
10. Sabate J, Bayona JM, Solanas AM. Photolysis of PAHs in aqueous phase by UV irradiation. Chemosphere. 2001; 44(2):119–24. [PubMed: 11444293]
11. Brame JA, Hong SW, Lee J, Lee SH, Alvarez PJ. Photocatalytic pre-treatment with food-grade TiO(2) increases the bioavailability and bioremediation potential of weathered oil from the Deepwater Horizon oil spill in the Gulf of Mexico. Chemosphere. 2013; 90(8):2315–9. [PubMed: 23177001]
12. Nicodem DE, Fernandes MCZ, Guedes CLB, Correa RJ. Photochemical processes and the environmental impact of petroleum spills. Biogeochemistry. 1997; 39(2):121–138.
13. Maki H, Sasaki T, Harayama S. Photo-oxidation of biodegraded crude oil and toxicity of the photo-oxidized products. Chemosphere. 2001; 44(5):1145–51. [PubMed: 11513402]
14. Lemkau KL, McKenna AM, Podgorski DC, Rodgers RP, Reddy CM. Molecular evidence of heavy-oil weathering following the M/V Cosco Busan spill: insights from Fourier transform ion cyclotron resonance mass spectrometry. Environ Sci Technol. 2014; 48(7):3760–7. [PubMed: 24559181]
15. Lea-Smith DJ, Biller SJ, Davey MP, Cotton CA, Sepulveda BMP, Turchyn AV, Scanlan DJ, Smith AG, Chisholm SW, Howe CJ. Contribution of cyanobacterial alkane production to the ocean hydrocarbon cycle. Proc Nat Acad Sci. 2015; 112(44):13591–13596. [PubMed: 26438854]
16. Valentine DL, Reddy CM. Latent hydrocarbons from cyanobacteria. Proc Nat Acad Sci. 2015; 112(44):13434–13435. [PubMed: 26483499]
17. Bacosa HP, Erdner DL, Liu Z. Differentiating the roles of photooxidation and biodegradation in the weathering of Light Louisiana Sweet crude oil in surface water from the Deepwater Horizon site. Mar Pollut Bull. 2015; 95(1):265–72. [PubMed: 25899525]
18. Lübcke-von Varel U, Machala M, Ciganek M, Neca J, Pencikova K, Palkova L, Vondracek J, Löffler I, Streck G, Reifferscheid G, Flückiger-Isler S, Weiss JM, Lamoree M, Brack W. Polar Compounds Dominate in Vitro Effects of Sediment Extracts. Environ Sci Technol. 2011; 45(6): 2384–2390. [PubMed: 21348526]
19. Lee RF. Photo-oxidation and photo-toxicity of crude and refined oils. Spill Sci Technol B. 2003; 8(2):157–162.
20. Duesterloh S, Short JW, Barron MG. Photoenhanced toxicity of weathered Alaska North Slope crude oil to the calanoid copepods Calanus marshallae and Metridia okhotensis. Environ Sci Technol. 2002; 36(18):3953–9. [PubMed: 12269748]
21. Barron MG, Carls MG, Heintz R, Rice SD. Evaluation of fish early life-stage toxicity models of chronic embryonic exposures to complex polycyclic aromatic hydrocarbon mixtures. Toxicol Sci. 2004; 78(1):60–7. [PubMed: 14691206]
22. Knecht AL, Goodale BC, Truong L, Simonich MT, Swanson AJ, Matzke MM, Anderson KA, Waters KM, Tanguay RL. Comparative developmental toxicity of environmentally relevant oxygenated PAHs. Toxicol Appl Pharmacol. 2013; 271(2):266–75. [PubMed: 23684558]

23. Huang XD, McConkey BJ, Babu TS, Greenberg BM. Mechanisms of photoinduced toxicity of photomodified anthracene to plants: Inhibition of photosynthesis in the aquatic higher plant Lemna gibba (duckweed). Environ Toxicol Chem. 1997; 16(8):1707–1715.
24. Duxbury CL, Dixon DG, Greenberg BM. Effects of simulated solar radiation on the bioaccumulation of polycyclic aromatic hydrocarbons by the duckweed Lemna gibba. Environ Toxicol Chem. 1997; 16(8):1739–1748.
25. Lampi MA, Gurska J, McDonald KI, Xie F, Huang XD, Dixon DG, Greenberg BM. Photoinduced toxicity of polycyclic aromatic hydrocarbons to Daphnia magna: ultraviolet-mediated effects and the toxicity of polycyclic aromatic hydrocarbon photoproducts. Environ Toxicol Chem. 2006; 25(4):1079–87. [PubMed: 16629147]
26. Mason OU, Scott NM, Gonzalez A, Robbins-Pianka A, Bælum J, Kimbrel J, Bouskill NJ, Prestat E, Borglin S, Joyner DC. Metagenomics reveals sediment microbial community response to Deepwater Horizon oil spill. ISME J. 2014; 8(7):1464–1475. [PubMed: 24451203]
27. Gong Y, Zhao X, Cai Z, O'Reilly SE, Hao X, Zhao D. A review of oil, dispersed oil and sediment interactions in the aquatic environment: Influence on the fate, transport and remediation of oil spills. Mari Pollut Bull. 2014; 79(1–2):16–33.
28. Boglaienko D, Tansel B. Partitioning of fresh crude oil between floating, dispersed and sediment phases: Effect of exposure order to dispersant and granular materials. J Environ Manag. 2016; 175:40–45.
29. Sandoval K, Ding Y, Gardinali P. Characterization and environmental relevance of oil water preparations of fresh and weathered MC-252 Macondo oils used in toxicology testing. Sci Total Environ. 2017; 576:118–128. [PubMed: 27783930]
30. King SM, Leaf PA, Olson AC, Ray PZ, Tarr MA. Photolytic and photocatalytic degradation of surface oil from the Deepwater Horizon spill. Chemosphere. 2014; 95(0):415–22. [PubMed: 24139429]
31. Radovic JR, Aeppli C, Nelson RK, Jimenez N, Reddy CM, Bayona JM, Albaiges J. Assessment of photochemical processes in marine oil spill fingerprinting. Mar Pollut Bull. 2014; 79(1–2):268–77. [PubMed: 24355571]
32. Faksness LG, Altin D, Nordtug T, Daling PS, Hansen BH. Chemical comparison and acute toxicity of water accommodated fraction (WAF) of source and field collected Macondo oils from the Deepwater Horizon spill. Mar Pollut Bull. 2015; 91(1):222–9. [PubMed: 25534626]
33. Theurich J, Bahnemann DW, Vogel R, Ehamed FE, Alhakimi G, Rajab I. Photocatalytic degradation of naphthalene and anthracene: GC-MS analysis of the degradation pathway. Res Chem Intermed. 1997; 23(3):247–274.
34. Rontani JF, Giral PJP. Significance of Photosensitized Oxidation of Alkanes during the Photochemical Degradation of Petroleum Hydrocarbon Fractions in Seawater. Int J Environ Anal Chem. 1990; 42(1–4):61–68.
35. Niederer M. Determination of polycyclic aromatic hydrocarbons and substitutes (nitro-, Oxy-PAHs) in urban soil and airborne particulate by GC-MS and NCI-MS/MS. Environ Sci Pollut Res Int. 1998; 5(4):209–16. [PubMed: 19002634]
36. Poster DL, Schantz MM, Sander LC, Wise SA. Analysis of polycyclic aromatic hydrocarbons (PAHs) in environmental samples: a critical review of gas chromatographic (GC) methods. Anal Bioanal Chem. 2006; 386(4):859–81. [PubMed: 17019586]
37. Webb PJ, Hamilton JF, Lewis AC, Wirtz K. Formation of oxygenated-polycyclic aromatic compounds in aerosol from the photo-oxidation of o-tolualdehyde. Polycyc Aromat Comp. 2006; 26(4):237–252.
38. McKenna AM, Nelson RK, Reddy CM, Savory JJ, Kaiser NK, Fitzsimmons JE, Marshall AG, Rodgers RP. Expansion of the analytical window for oil spill characterization by ultrahigh resolution mass spectrometry: beyond gas chromatography. Environ Sci Technol. 2013; 47(13): 7530–9. [PubMed: 23692145]
39. Forth HP, Mitchelmore CL, Morris JM, Lipton J. Characterization of oil and water accommodated fractions used to conduct aquatic toxicity testing in support of the Deepwater Horizon oil spill natural resource damage assessment. Environ Toxicol Chem. 2016; doi: 10.1002/etc.3672

40. Rowland S, Donkin P, Smith E, Wraige E. Aromatic Hydrocarbon “Humps” in the Marine Environment: Unrecognized Toxins? Environ Sci Technol. 2001; 35(13):2640–2644. [PubMed: 11452586]

41. Ray PZ, Chen H, Podgorski DC, McKenna AM, Tarr MA. Sunlight creates oxygenated species in water-soluble fractions of Deepwater Horizon oil. J Hazard Mater. 2014; 280(0):636–43. [PubMed: 25222929]

42. Ruddy BM, Huettel M, Kostka JE, Lobodin VV, Bythell BJ, McKenna AM, Aeppli C, Reddy CM, Nelson RK, Marshall AG, Rodgers RP. Targeted Petroleomics: Analytical Investigation of Macondo Well Oil Oxidation Products from Pensacola Beach. Energy Fuels. 2014; 28(6):4043–4050.

43. Griffiths MT, Da Campo R, O’Connor PB, Barrow MP. Throwing light on petroleum: simulated exposure of crude oil to sunlight and characterization using atmospheric pressure photoionization fourier transform ion cyclotron resonance mass spectrometry. Anal Chem. 2014; 86(1):527–34. [PubMed: 24328063]

44. Islam A, Cho Y, Yim UH, Shim WJ, Kim YH, Kim S. The comparison of naturally weathered oil and artificially photo-degraded oil at the molecular level by a combination of SARA fractionation and FT-ICR MS. J Hazard Mater. 2013; 263(Pt 2, (0)):404–11. [PubMed: 24231315]

45. Zhu X, Shi Q, Zhang Y, Pan N, Xu C, Chung KH, Zhao S. Energy Fuels. 2011; 25:281.

46. Molnárné Guricza L, Schrader W. Electrospray ionization for determination of non-polar polyaromatic hydrocarbons and polyaromatic heterocycles in heavy crude oil asphaltenes. J Mass Spectrom. 2015; 50(3):549–557. [PubMed: 25800191]

47. Hourani N, Andersson JT, Möller I, Amad MA, Witt M, Sarathy SM. Atmospheric pressure chemical ionization Fourier transform ion cyclotron resonance mass spectrometry for complex thiophenic mixture analysis. Rapid Commun Mass Spectrom. 2013; 27(21):2432–2438. [PubMed: 24097400]

48. Barrow MP, Peru KM, Headley JV. An added dimension: GC atmospheric pressure chemical ionization FTICR MS and the Athabasca oil sands. Anal Chem. 2014; 86(16):8281–8288. [PubMed: 25036898]

49. Headley JV, Peru KM, Barrow MP. Advances in mass spectrometric characterization of naphthenic acids fraction compounds in oil sands environmental samples and crude oil—a review. Mass Spectrom Rev. 2016; 35(2):311–328. [PubMed: 25970647]

50. Headley JV, Peru KM, Mohamed MH, Wilson L, McMartin DW, Mapolelo MM, Lobodin VV, Rodgers RP, Marshall AG. Atmospheric Pressure Photoionization Fourier Transform Ion Cyclotron Resonance Mass Spectrometry Characterization of Tunable Carbohydrate-Based Materials for Sorption of Oil Sands Naphthenic Acids. Energy Fuels. 2013; 28(3):1611–1616.

51. Bae E, Na JG, Chung SH, Kim HS, Kim S. Identification of about 30000 chemical components in shale oils by electrospray ionization (ESI) and atmospheric pressure photoionization (APPI) coupled with 15 T Fourier transform ion cyclotron resonance mass spectrometry (FT-ICR MS) and a comparison to conventional oil. Energy Fuels. 2010; 24(4):2563–2569.

52. Corilo YE, Rowland SM, Rodgers RP. Calculation of the total sulfur content in crude oils by positive-ion atmospheric pressure photoionization Fourier transform ion cyclotron resonance mass spectrometry. Energy Fuels. 2016; 30(5):3962–3966.

53. Vetere A, Schrader W. Mass Spectrometric Coverage of Complex Mixtures: Exploring the Carbon Space of Crude Oil. ChemistrySelect. 2017; 2(3):849–853.

54. Stader C, Beer FT, Achten C. Environmental PAH analysis by gas chromatography–atmospheric pressure laser ionization–time-of-flight–mass spectrometry (GC-APLI-MS). Anal Bioanal Chem. 2013; 405(22):7041–7052. [PubMed: 23852149]

55. Schmitt-Kopplin P, Englmann M, Rossello-Mora R, Schiewek R, Brockmann KJ, Benter T, Schmitz OJ. Combining chip-ESI with APLI (cESILI) as a multimode source for analysis of complex mixtures with ultrahigh-resolution mass spectrometry. Anal Bioanal Chem. 2008; 391(8):2803–2809. [PubMed: 18566804]

56. Schiewek R, Schellenträger M, Mönnikes R, Lorenz M, Giese R, Brockmann K, Gäb S, Benter T, Schmitz O. Ultrasensitive determination of polycyclic aromatic compounds with atmospheric-

pressure laser ionization as an interface for GC/MS. Anal Chem. 2007; 79(11):4135–4140. [PubMed: 17472342]

57. Streibel T, Zimmermann R. Resonance-Enhanced Multiphoton Ionization Mass Spectrometry (REMPI-MS): Applications for Process Analysis. Annu Rev Anal Chem. 2014; 7(1):361–381.
58. Gaspar A, Zellermann E, Lababidi S, Reece J, Schrader W. Characterization of Saturates, Aromatics, Resins, and Asphaltenes Heavy Crude Oil Fractions by Atmospheric Pressure Laser Ionization Fourier Transform Ion Cyclotron Resonance Mass Spectrometry. Energy Fuels. 2012; 26(6):3481–3487.
59. Lababidi S, Panda SK, Andersson JT, Schrader W. Direct coupling of normal-phase high-performance liquid chromatography to atmospheric pressure laser ionization fourier transform ion cyclotron resonance mass spectrometry for the characterization of crude oil. Anal Chem. 2013; 85(20):9478–85. [PubMed: 24063573]
60. Lababidi S, Schrader W. Online normal-phase high-performance liquid chromatography/Fourier transform ion cyclotron resonance mass spectrometry: effects of different ionization methods on the characterization of highly complex crude oil mixtures. Rapid Commun Mass Spectrom. 2014; 28(12):1345–52. [PubMed: 24797945]
61. Panda SK, Brockmann KJ, Benter T, Schrader W. Atmospheric pressure laser ionization (APLI) coupled with Fourier transform ion cyclotron resonance mass spectrometry applied to petroleum samples analysis: comparison with electrospray ionization and atmospheric pressure photoionization methods. Rapid Commun Mass Spectrom. 2011; 25(16):2317–2326. [PubMed: 21769956]
62. Huba AK, Huba K, Gardinali PR. Understanding the atmospheric pressure ionization of petroleum components: The effects of size, structure, and presence of heteroatoms. Sci Total Environ. 2016; 568:1018–1025. [PubMed: 27363346]
63. Cho Y, Ahmed A, Islam A, Kim S. Developments in FT-ICR MS instrumentation, ionization techniques, and data interpretation methods for petroleomics. Mass Spectrom Rev. 2015; 34(2): 248–263. [PubMed: 24942384]
64. Pudenzi MA, Eberlin MN. Assessing Relative Electrospray Ionization, Atmospheric Pressure Photoionization, Atmospheric Pressure Chemical Ionization, and Atmospheric Pressure Photo- and Chemical Ionization Efficiencies in Mass Spectrometry Petroleomic Analysis via Pools and Pairs of Selected Polar Compound Standards. Energy Fuels. 2016; 30(9):7125–7133.
65. Benigni P, DeBord JD, Thompson CJ, Gardinali P, Fernandez-Lima F. Increasing Polyaromatic Hydrocarbon (PAH) Molecular Coverage during Fossil Oil Analysis by Combining Gas Chromatography and Atmospheric-Pressure Laser Ionization Fourier Transform Ion Cyclotron Resonance Mass Spectrometry (FT-ICR MS). Energy Fuels. 2016; 30(1):196–203. [PubMed: 27212790]
66. Molnárné Guricza L, Schrader W. New Separation Approach for Asphaltene Investigation: Argentation Chromatography Coupled with Ultrahigh-Resolution Mass Spectrometry. Energy Fuels. 2015; 29(10):6224–6230.
67. Ghislain T, Molnarne Guricza L, Schrader W. Characterization of crude oil asphaltenes by coupling size exclusion chromatography directly to an ultrahigh resolution mass spectrometer. Rapid Commun Mass Spectrom. 2017; 31(6):495–502. [PubMed: 28010034]
68. Ramirez CE, Wang C, Gardinali PR. Fully automated trace level determination of parent and alkylated PAHs in environmental waters by online SPE-LC-APPI-MS/MS. Anal Bioanal Chem. 2014; 406(1):329–344. [PubMed: 24217946]
69. Rüger CP, Schwemer T, Sklorz M, O'Connor PB, Barrow MP, Zimmermann R. Comprehensive chemical comparison of fuel composition and aerosol particles emitted from a ship diesel engine by gas chromatography atmospheric pressure chemical ionisation ultra-high resolution mass spectrometry with improved data processing routines. Eur J Mass Spectrom. 2017; doi: 10.1177/1469066717694286
70. Vetere A, Schrader W. 1-and 2-Photon ionization for online FAIMS-FTMS coupling allows new insights into the constitution of crude oils. Anal Chem. 2015; 87(17):8874–8879. [PubMed: 26221748]

71. Ibrahim YM, Garimella SV, Prost SA, Wojcik R, Norheim RV, Baker ES, Rusyn I, Smith RD. Development of an Ion Mobility Spectrometry-Orbitrap Mass Spectrometer Platform. Anal Chem. 2016; 88(24):12152–12160. [PubMed: 28193022]
72. Kailemia MJ, Park M, Kaplan DA, Venot A, Boons GJ, Li L, Linhardt RJ, Amster IJ. High-field asymmetric-waveform ion mobility spectrometry and electron detachment dissociation of isobaric mixtures of glycosaminoglycans. J Am Soc Mass Spectrom. 2014; 25(2):258–68. [PubMed: 24254578]
73. Robinson EW, Garcia DE, Leib RD, Williams ER. Enhanced mixture analysis of poly(ethylene glycol) using high-field asymmetric waveform ion mobility spectrometry combined with fourier transform ion cyclotron resonance mass spectrometry. Anal Chem. 2006; 78(7):2190–8. [PubMed: 16579597]
74. Robinson EW, Leib RD, Williams ER. The role of conformation on electron capture dissociation of ubiquitin. J Am Soc Mass Spectrom. 2006; 17(10):1469–79. [PubMed: 16890453]
75. Robinson EW, Sellon RE, Williams ER. Peak deconvolution in high-field asymmetric waveform ion mobility spectrometry (FAIMS) to characterize macromolecular conformations. Int J Mass Spectrom. 2007; 259(1–3):87–95. [PubMed: 19079801]
76. Robinson EW, Williams ER. Multidimensional separations of ubiquitin conformers in the gas phase: relating ion cross sections to H/D exchange measurements. J Am Soc Mass Spectrom. 2005; 16(9):1427–37. [PubMed: 16023362]
77. Tang X, Bruce JE, Hill HH Jr. Design and performance of an atmospheric pressure ion mobility Fourier transform ion cyclotron resonance mass spectrometer. Rapid Commun Mass Spectrom. 2007; 21(7):1115–22. [PubMed: 17318922]
78. Bluhm BK, Gillig KJ, Russell DH. Development of a Fourier-transform ion cyclotron resonance mass spectrometer-ion mobility spectrometer. Rev Sci Instrum. 2000; 71(11):4078–4086.
79. Benigni P, Thompson CJ, Ridgeway ME, Park MA, Fernandez-Lima F. Targeted high-resolution ion mobility separation coupled to ultrahigh-resolution mass spectrometry of endocrine disruptors in complex mixtures. Anal Chem. 2015; 87(8):4321–5. [PubMed: 25818070]
80. Wu C, Siems WF, Asbury GR, Hill HH. Electrospray Ionization High-Resolution Ion Mobility Spectrometry−Mass Spectrometry. Anal Chem. 1998; 70(23):4929–4938. [PubMed: 21644676]
81. Jarrold MF, Constant VA. Silicon cluster ions: evidence for a structural transition. Phys Rev Lett. 1991; 67(21):2994. [PubMed: 10044611]
82. Kanu AB, Dwivedi P, Tam M, Matz L, Hill HH. Ion mobility–mass spectrometry. J Mass Spectrom. 2008; 43(1):1–22. [PubMed: 18200615]
83. Becker C, Qian K, Russell DH. Molecular Weight Distributions of Asphaltenes and Deasphaltened Oils Studied by Laser Desorption Ionization and Ion Mobility Mass Spectrometry. Anal Chem. 2008; 80(22):8592–8597. [PubMed: 18937419]
84. Lalli PM, Corilo YE, Rowland SM, Marshall AG, Rodgers RP. Isomeric Separation and Structural Characterization of Acids in Petroleum by Ion Mobility Mass Spectrometry. Energy Fuels. 2015; 29(6):3626–3633.
85. Fasciotti M, Lalli PM, Klitzke CF, Corilo YE, Pudenzi MA, Pereira RCL, Bastos W, Daroda RJ, Eberlin MN. Petroleomics by Traveling Wave Ion Mobility-Mass Spectrometry Using CO2 as a Drift Gas. Energy Fuels. 2013; 27(12):7277–7286.
86. Fernandez-Lima FA, Becker C, McKenna AM, Rodgers RP, Marshall AG, Russell DH. Petroleum crude oil characterization by IMS-MS and FTICR MS. Anal Chem. 2009; 81(24):9941–7. [PubMed: 19904990]
87. Becker C, Fernandez-Lima FA, Russell DH. Ion Mobility-Mass Spectrometry: A Tool for Characterizing the Petroleome. Spectroscopy. 2009; 24(4):38–42.
88. Ahmed A, Cho Y, Giles K, Riches E, Lee JW, Kim HI, Choi CH, Kim S. Elucidating Molecular Structures of Nonalkylated and Short-Chain Alkyl (n < 5, (CH2)n) Aromatic Compounds in Crude Oils by a Combination of Ion Mobility and Ultrahigh-Resolution Mass Spectrometries and Theoretical Collisional Cross-Section Calculations. Anal Chem. 2014; 86(7):3300–3307. [PubMed: 24592806]

89. Ahmed A, Cho YJ, No M-h, Koh J, Tomczyk N, Giles K, Yoo JS, Kim S. Application of the Mason−Schamp Equation and Ion Mobility Mass Spectrometry To Identify Structurally Related Compounds in Crude Oil. Anal Chem. 2010; 83(1):77–83. [PubMed: 21117627]

90. Farenc M, Corilo YE, Lalli PM, Riches E, Rodgers RP, Afonso C, Giusti P. Comparison of Atmospheric Pressure Ionization for the Analysis of Heavy Petroleum Fractions with Ion Mobility-Mass Spectrometry. Energy Fuels. 2016; 30(11):8896–8903.

91. Santos JM, Galaverna RdS, Pudenzi MA, Schmidt EM, Sanders NL, Kurulugama RT, Mordehai A, Stafford GC, Wisniewski A, Eberlin MN. Petroleomics by ion mobility mass spectrometry: resolution and characterization of contaminants and additives in crude oils and petrofuels. Anal Meth. 2015; 7(11):4450–4463.

92. Lalli PM, Jarvis JM, Marshall AG, Rodgers RP. Functional Isomers in Petroleum Emulsion Interfacial Material Revealed by Ion Mobility Mass Spectrometry and Collision-Induced Dissociation. Energy Fuels. 2017

93. Hernandez DR, Debord JD, Ridgeway ME, Kaplan DA, Park MA, Fernandez-Lima F. Ion dynamics in a trapped ion mobility spectrometer. Analyst. 2014; 139(8):1913–21. [PubMed: 24571000]

94. Fernandez-Lima FA, Kaplan DA, Park MA. Note: Integration of trapped ion mobility spectrometry with mass spectrometry. Rev Sci Instrum. 2011; 82(12):126106. [PubMed: 22225261]

95. Fernandez-Lima F, Kaplan DA, Suetering J, Park MA. Gas-phase separation using a trapped ion mobility spectrometer. Int J Ion Mobil Spectrom. 2011; 14(2–3):93–98.

96. Castellanos A, Benigni P, Hernandez DR, DeBord JD, Ridgeway ME, Park MA, Fernandez-Lima F. Fast Screening of Polycyclic Aromatic Hydrocarbons using Trapped Ion Mobility Spectrometry - Mass Spectrometry. Anal Meth. 2014; 6(23):9328–9332.

97. Benigni P, Marin R, Fernandez-Lima F. Towards unsupervised polyaromatic hydrocarbons structural assignment from SA-TIMS-FTMS data. Int J Ion Mobil Spectrom. 2015; 18(3):151–157. [PubMed: 26525904]

98. Schenk ER, Mendez V, Landrum JT, Ridgeway ME, Park MA, Fernandez-Lima F. Direct observation of differences of carotenoid polyene chain cis/trans isomers resulting from structural topology. Anal Chem. 2014; 86(4):2019–24. [PubMed: 24428664]

99. Schenk ER, Ridgeway ME, Park MA, Leng F, Fernandez-Lima F. Isomerization kinetics of AT hook decapeptide solution structures. Anal Chem. 2014; 86(2):1210–4. [PubMed: 24364733]

100. Schenk ER, Nau F, Fernandez-Lima F. Theoretical predictor for candidate structure assignment from IMS data of biomolecule-related conformational space. Int J Ion Mobil Spectrom. 2015; 18(1):23–29. [PubMed: 27330407]

101. Schenk ER, Almeida R, Miksovska J, Ridgeway ME, Park MA, Fernandez-Lima F. Kinetic intermediates of holo- and apo-myoglobin studied using HDX-TIMS-MS and molecular dynamic simulations. J Am Soc Mass Spectrom. 2015; 26(4):555–63. [PubMed: 25690175]

102. Benigni P, Marin R, Molano-Arevalo JC, Garabedian A, Wolff JJ, Ridgeway ME, Park MA, Fernandez-Lima F. Towards the Analysis of High Molecular Weight Proteins and Protein complexes using TIMS-MS. Int J Ion Mobil Spectrom. 2016; 19(2):95–104. [PubMed: 27818614]

103. Garabedian A, Butcher D, Lippens JL, Miksovska J, Chapagain PP, Fabris D, Ridgeway ME, Park MA, Fernandez-Lima F. Structures of the kinetically trapped i-motif DNA intermediates. Phys Chem Chem Phys. 2016; 18(38):26691–26702. [PubMed: 27711445]

104. Molano-Arevalo JC, Hernandez DR, Gonzalez WG, Miksovska J, Ridgeway ME, Park MA, Fernandez-Lima F. Flavin adenine dinucleotide structural motifs: from solution to gas phase. Anal Chem. 2014; 86(20):10223–30. [PubMed: 25222439]

105. McKenzie-Coe A, DeBord JD, Ridgeway M, Park M, Eiceman G, Fernandez-Lima F. Lifetimes and stabilities of familiar explosive molecular adduct complexes during ion mobility measurements. Analyst. 2015; 140(16):5692–9. [PubMed: 26153567]

106. Benigni P, Fernandez-Lima F. Oversampling Selective Accumulation Trapped Ion Mobility Spectrometry Coupled to FT-ICR MS: Fundamentals and Applications. Anal Chem. 2016; 88(14):7404–12. [PubMed: 27340830]

107. Adams KJ, Montero D, Aga D, Fernandez-Lima F. Isomer separation of polybrominated diphenyl ether metabolites using nanoESI-TIMS-MS. Int J Ion Mobil Spectrom. 2016; 19(2):69–76. [PubMed: 27642261]
108. Silveira JA, Ridgeway ME, Laukien FH, Mann M, Park MA. Parallel accumulation for 100% duty cycle trapped ion mobility-mass spectrometry. Int J Mass Spectrom. 2017; 413:168–175.
109. Michelmann K, Silveira JA, Ridgeway ME, Park MA. Fundamentals of Trapped Ion Mobility Spectrometry. J Am Soc Mass Spectrom. 2015; 26(1):14–24. [PubMed: 25331153]
110. Silveira JA, Michelmann K, Ridgeway ME, Park MA. Fundamentals of Trapped Ion Mobility Spectrometry Part II: Fluid Dynamics. J Am Soc Mass Spectrom. 2016; 27(4):585–595. [PubMed: 26864793]
111. Silveira JA, Danielson W, Ridgeway ME, Park MA. Altering the mobility-time continuum: nonlinear scan functions for targeted high resolution trapped ion mobility-mass spectrometry. Int J Ion Mobil Spectrom. 2016; 19(2):87–94.
112. Ridgeway ME, Silveira JA, Meier JE, Park MA. Microheterogeneity within conformational states of ubiquitin revealed by high resolution trapped ion mobility spectrometry. Analyst. 2015; 140(20):6964–6972. [PubMed: 26106655]
113. Meier F, Beck S, Grassl N, Lubeck M, Park MA, Raether O, Mann M. Parallel Accumulation–Serial Fragmentation (PASEF): Multiplying Sequencing Speed and Sensitivity by Synchronized Scans in a Trapped Ion Mobility Device. J Proteome Res. 2015; 14(12):5378–5387. [PubMed: 26538118]
114. Silveira JA, Ridgeway ME, Park MA. High Resolution Trapped Ion Mobility Spectrometery of Peptides. Anal Chem. 2014; 86(12):5624–5627. [PubMed: 24862843]
115. Ridgeway ME, Wolff JJ, Silveira JA, Lin C, Costello CE, Park MA. Gated trapped ion mobility spectrometry coupled to fourier transform ion cyclotron resonance mass spectrometry. Int J Ion Mobil Spectrom. 2016; 19(2):77–85. [PubMed: 27667964]
116. Pu Y, Ridgeway ME, Glaskin RS, Park MA, Costello CE, Lin C. Separation and Identification of Isomeric Glycans by Selected Accumulation-Trapped Ion Mobility Spectrometry-Electron Activated Dissociation Tandem Mass Spectrometry. Anal Chem. 2016; 88(7):3440–3443. [PubMed: 26959868]
117. Liu FC, Kirk SR, Bleiholder C. On the structural denaturation of biological analytes in trapped ion mobility spectrometry–mass spectrometry. Analyst. 2016; 141(12):3722–3730. [PubMed: 26998732]
118. Lundstedt S, White PA, Lemieux CL, Lynes KD, Lambert LB, Oberg L, Haglund P, Tysklind M. Sources, fate, and toxic hazards of oxygenated polycyclic aromatic hydrocarbons (PAHs) at PAH-contaminated sites. Ambio. 2007; 36(6):475–485. [PubMed: 17985702]
119. Singer MM, Aurand D, Bragin GE, Clark JR, Coelho GM, Sowby ML, Tjeerdema RS. Standardization of the preparation and quantitation of water-accommodated fractions of petroleum for toxicity testing. Mari Pollut Bull. 2000; 40(11):1007–1016.
120. Benigni P, Marin R, Sandoval K, Gardinali P, Fernandez-Lima F. Chemical Analysis of Water-accommodated Fractions of Crude Oil Spills Using TIMS-FT-ICR MS. J Vis Exp. 2017; 121:e55352.
121. McDaniel, EW., Mason, EA. Mobility and diffusion of ions in gases. John Wiley and Sons, Inc; New York: New York: 1973. p. 381
122. Savory JJ, Kaiser NK, McKenna AM, Xian F, Blakney GT, Rodgers RP, Hendrickson CL, Marshall AG. Parts-per-billion Fourier transform ion cyclotron resonance mass measurement accuracy with a “walking” calibration equation. Anal Chem. 2011; 83(5):1732–1736. [PubMed: 21275417]
123. Du P, Kibbe WA, Lin SM. Improved peak detection in mass spectrum by incorporating continuous wavelet transform-based pattern matching. Bioinformatics. 2006; 22(17):2059–2065. [PubMed: 16820428]
124. Oliphant TE. Python for Scientific Computing. Comput Sci Eng. 2007; 9(3):10–20.
125. Moré JJ, Garbow BS, Hillstrom KE. User guide for MINPACK-1. 1980 CM-P00068642.
126. Hunter JD. Matplotlib: A 2D graphics environment. Comput Sci Eng. 2007; 9(3):90–95.

127. Fasciotti M, Lalli PM, Heerdt G, Steffen RA, Corilo YE, de Sá GF, Daroda RJ, Reis FdAM, Morgon NH, Pereira RCL, Eberlin MN, Klitzke CF. Structure-drift time relationships in ion mobility mass spectrometry. Int J Ion Mobil Spectrom. 2013; 16(2):117–132.

128. Dabestani R, Ivanov IN. A compilation of physical, spectroscopic and photo physical properties of polycyclic aromatic hydrocarbons. Photochem Photobiol. 1999; 70(1):10–34.

129. Chen H, Hou A, Corilo YE, Lin Q, Lu J, Mendelssohn IA, Zhang R, Rodgers RP, McKenna AM. 4 Years after the Deepwater Horizon Spill: Molecular Transformation of Macondo Well Oil in Louisiana Salt Marsh Sediments Revealed by FT-ICR Mass Spectrometry. Environ Sci Technol. 2016; 50(17):9061–9069. [PubMed: 27465015]

130. Leshuk T, Wong T, Linley S, Peru KM, Headley JV, Gu F. Solar photocatalytic degradation of naphthenic acids in oil sands process-affected water. Chemosphere. 2016; 144:1854–1861. [PubMed: 26539710]

131. Huba AK, Gardinali PR. Characterization of a crude oil weathering series by ultrahigh-resolution mass spectrometry using multiple ionization modes. Sci Total Environ. 2016; 563–564:600–610.

132. van Agthoven MA, Delsuc MA, Rolando C. Two-dimensional FT-ICR/MS with IRMPD as fragmentation mode. Int J Mass Spectrom. 2011; 306(2):196–203.

133. Laskin, J. Principles of Mass Spectrometry Applied to Biomolecules. John Wiley & Sons, Inc; 2006. Energy and Entropy Effects in Gas-Phase Dissociation of Peptides and Proteins; p. 619-665.

134. Klassen JS, Schnier PD, Williams ER. Blackbody infrared radiative dissociation of oligonucleotide anions. J Am Soc Mass Spectrom. 1998; 9(11):1117–24. [PubMed: 9794082]

135. Felitsyn N, Kitova EN, Klassen JS. Thermal decomposition of a gaseous multiprotein complex studied by blackbody infrared radiative dissociation. Investigating the origin of the asymmetric dissociation behavior. Anal Chem. 2001; 73(19):4647–61. [PubMed: 11605843]

136. Dunbar RC. BIRD (blackbody infrared radiative dissociation): evolution, principles, and applications. Mass Spectrom Rev. 2004; 23(2):127–58. [PubMed: 14732935]

137. Yan J, Zhou M, Gilbert JD, Wolff JJ, Somogyi A, Pedder RE, Quintyn RS, Morrison LJ, Easterling ML, Paša-Tolić L. Surface-induced dissociation (SID) of protein complexes in a hybrid Fourier transform ion cyclotron resonance (FT-ICR) mass spectrometer. Anal Chem. 2017; 89(1):895–901. [PubMed: 27977147]

138. Qi Y, Volmer DA. Structural analysis of small to medium-sized molecules by mass spectrometry after electron-ion fragmentation (ExD) reactions. Analyst. 2016; 141(3):794–806. [PubMed: 26725919]

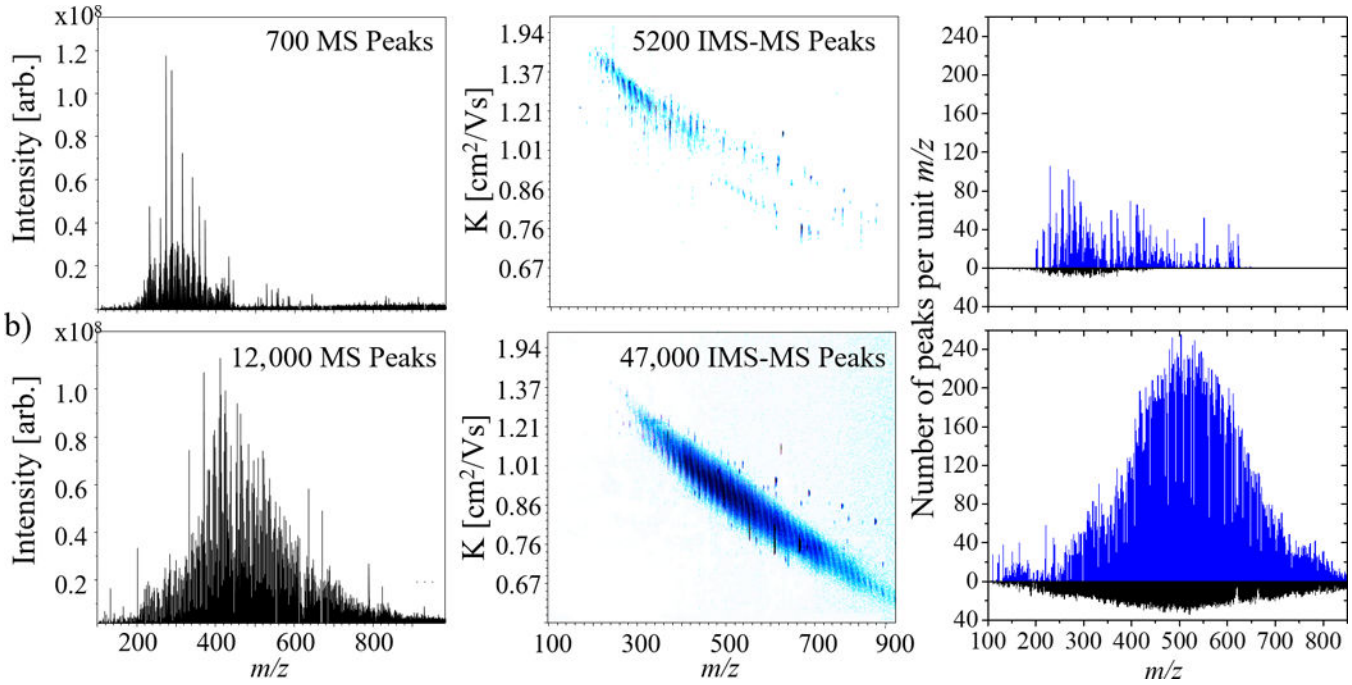

Figure 1.

Typical FT-ICR MS spectrum and 2D TIMS-FT-ICR MS contour plot for the WAF (a) at 0, and (b) 115h light exposed. The number of peaks identified per unit *m/z* in the MS domain (black) and TIMS-MS (blue) domains are also shown for (a) and (b). Notice the significant differences in the number of identifications between (a) and (b), as well as between the MS and TIMS MS experiments, increasing the level of molecular feautres identified per analysis.

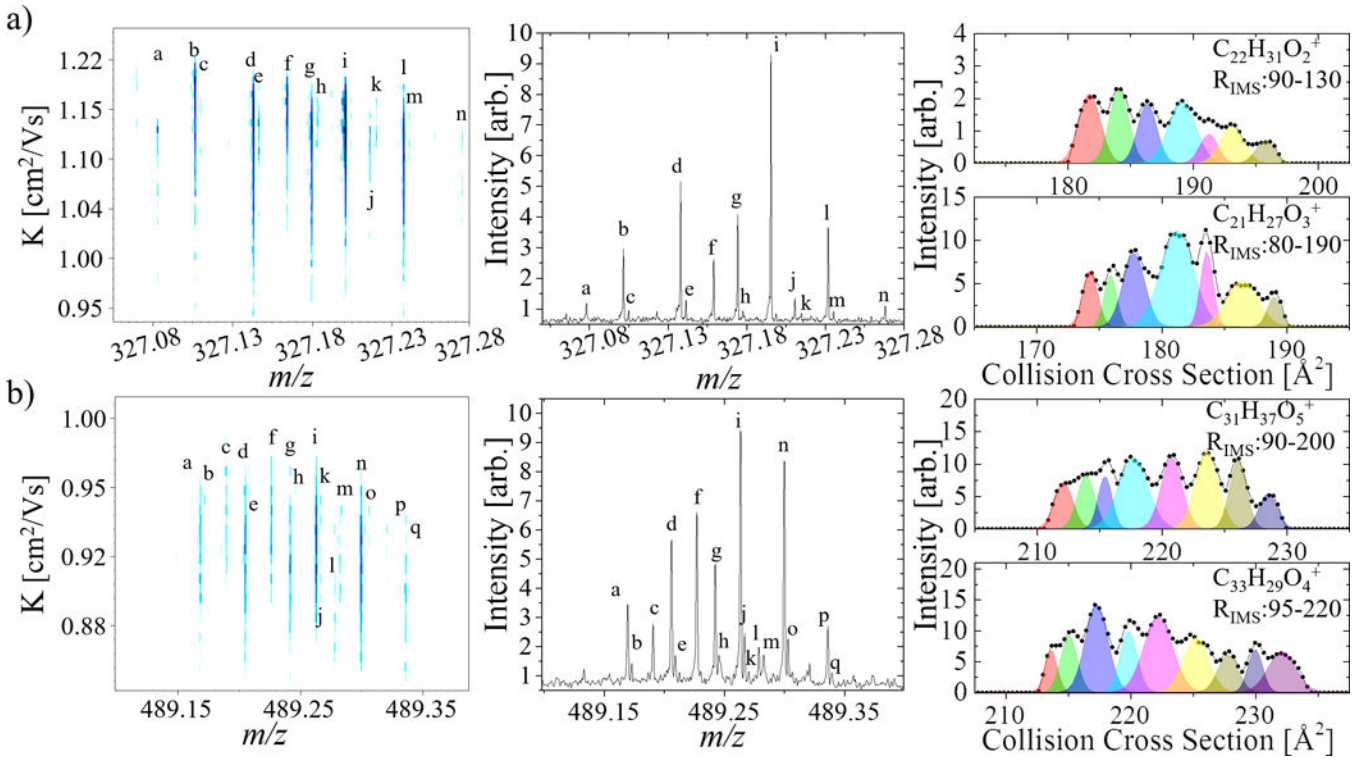

Figure 2.

Typical 2D TIMS-FT-ICR MS contour plot and MS projections for *m/z* a) 327 and b) 489. IMS projections for specific chemical formulas (connected scatterplot) with the unsupervised fitting by SAME package of minimum number of mobility features is shown. Note that the SAME package relies on the experimental profile of the distribution, which is able to show multiple features due to the high resolving power of the TIMS analyzer. Formula assignments are provided in table 1.

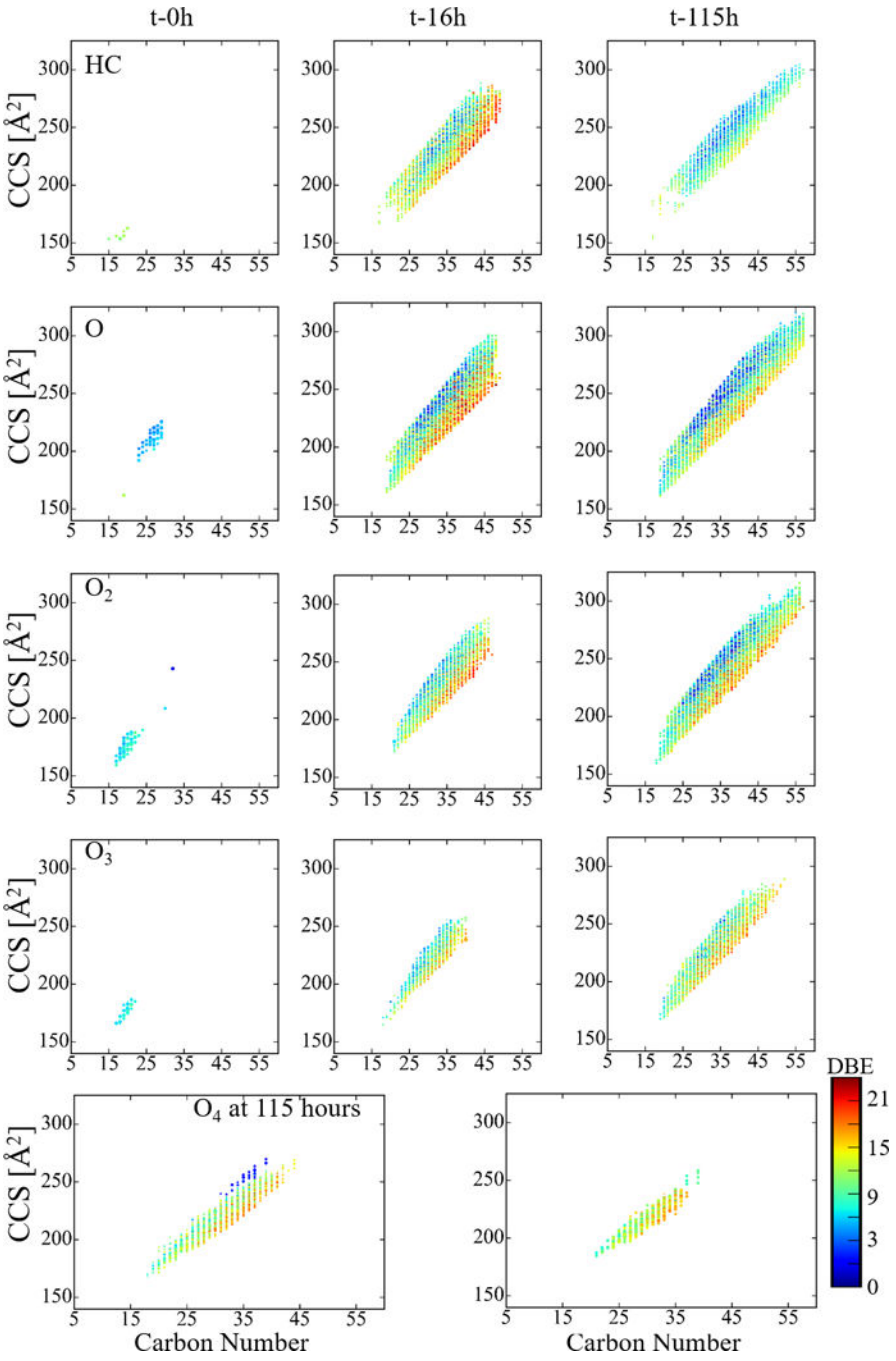

Figure 3.

Typical size dependence (CCS) with carbon number for the $O_{0\text{-}4}$ chemical classes observed in the WAF samples as a function to exposure to light (t-0, 16 and 115h). The color scale corresponds to the number of rings and double bond equivalents (DBE) of a molecule. Note the large increase in assignments between t-0h and t-16h, as well as increases in oxygen content between t-16h and t-115h.

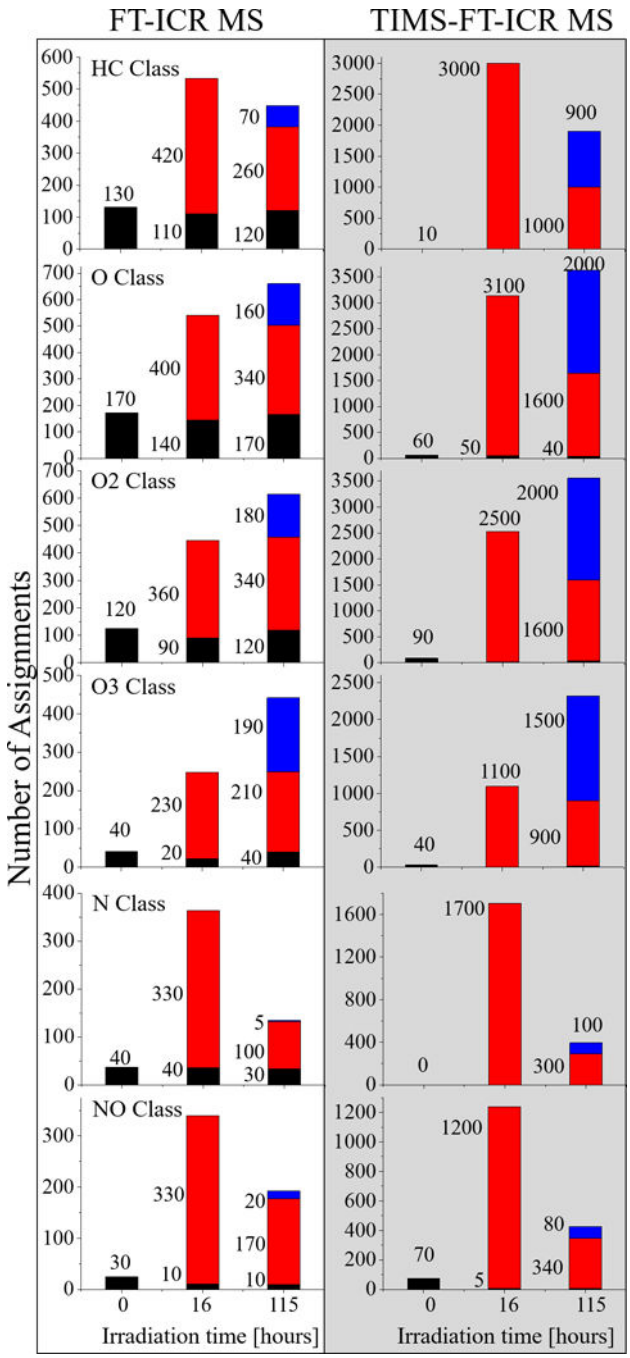

Figure 4.

Total number of molecular feature assignments based on chemical formula alone from FT-ICR MS measurements and based on chemical formula and IMS profiling from TIMS-FT-ICR MS measurements . Identifications unique to t-0, t-16, and t-115h are in black, red, and blue, respectively. When using FT-ICR MS is used tracing the evolution of the chemical complexity is incomplete, because the isomeric complexity is not taken into account. Particularly, taking into account the isomeric variability indicates that the composition of the

WAF at t-115h is significantly more complex, and chemically unique, than is observed by FT-ICR MS alone.

Table 1

Table of identified ion formulas for *m/z* 327 and 489 as found in figure 2.

m/z		Exp. m/z	Ion Formula	Error (ppb)
327	a	327.078031	$C_{15}H_{21}NOS_3^+$	−159
	b	327.101557	$C_{22}H_{15}O_3^+$	43
	c	327.104917	$C_{19}H_{19}O_3S^+$	76
	d	327.137957	$C_{23}H_{19}O_2$	−3
	e	327.141345	$C_{20}H_{23}O_2S^+$	−55
	f	327.159052	$C_{20}H_{23}O_4^+$	104
	g	327.174325	$C_{24}H_{23}O^+$	52
	h	327.177623	$C_{21}H_{27}OS^+$	275
	i	327.195425	$C_{21}H_{27}O_3^+$	141
	j	327.210673	$C_{25}H_{27}^+$	165
	k	327.214774	$C_{22}H_{31}S^+$	−2066
	l	327.231822	$C_{22}H_{31}O_2^+$	107
	m	327.235269	$C_{19}H_{35}O_2S$	−125
	n	327.268202	$C_{23}H_{35}O^+$	122
489	a	489.169661	$C_{32}H_{25}O_5^+$	−22
	b	489.172941	$C_{29}H_{29}O_5S^+$	164
	c	489.190592	$C_{29}H_{29}O_7$	384
	d	489.205937	$C_{33}H_{29}O_4^+$	202
	e	489.209127	$C_{30}H_{33}O_4S^+$	572
	f	489.227101	$C_{30}H_{33}O_6^+$	131
	g	489.242320	$C_{34}H_{33}O_3^+$	206
	h	489.245496	$C_{31}H_{37}O_3S^+$	605
	i	489.263445	$C_{31}H_{37}O_5^+$	217
	j	489.266855	$C_{28}H_{41}O_5S^+$	137
	k	489.270311	$C_{25}H_{45}O_5S_2^+$	−37
	l	489.278685	$C_{35}H_{37}O_2^+$	249
	m	489.282768	$C_{32}H_{41}O_2S^+$	−1206
	n	489.299809	$C_{32}H_{41}O_4^+$	260
	o	489.302875	$C_{29}H_{45}O_4S^+$	883
	p	489.336155	$C_{33}H_{45}O_3^+$	341
	q	489.339652	$C_{30}H_{49}O_3S^+$	84